New physics model in GEANT4 for the simulation of neutron interactions with organic scintillation detectors

CrossMark

A.R. Garcia [a], E. Mendoza [a], D. Cano-Ott [a,*], R. Nolte [b], T. Martinez [a], A. Algora [c,d], J.L. Tain [c], K. Banerjee [e], C. Bhattacharya [e]

[a] Centro de Investigaciones Energéticas, Medioambientales y Tecnológicas (CIEMAT), Avenida Complutense 40, Madrid 28040, Spain
[b] Physikalisch-Technische Bundesanstalt (PTB), Bundesallee 100, Braunschweig D-38116, Germany
[c] Instituto de Física Corpuscular (IFIC), CSIC–Universidad de Valencia, Valencia 46071, Spain
[d] Institute of Nuclear Research of the Hungarian Academy of Sciences (ATOMKI), Debrecen H-4026, Hungary
[e] Variable Energy Cyclotron Centre (VECC), 1/AF, Bidhannagar, Kolkata 700064, India

A R T I C L E   I N F O

A B S T R A C T

The accurate determination of the response function of organic scintillation neutron detectors complements their experimental characterization. Monte Carlo simulations with GEANT4 can reduce the effort and cost implied, especially for complex detection systems for which the characterization is more challenging. Previous studies have reported on the inaccuracy of GEANT4 in the calculation of the neutron response of organic scintillation detectors above 6 MeV, due to an incomplete description of the neutron-induced alpha production reactions on carbon. We have improved GEANT4 in this direction by incorporating models and data from NRESP, an excellent Monte Carlo simulation tool developed at the Physikalisch-Technische Bundesanstalt (PTB), Germany, for the specific purpose of calculating the neutron response function of organic scintillation detectors. The results have been verified against simulations with NRESP and validated against Time-Of-Flight measurements with an NE213 detector at PTB. This work has potential applications beyond organic scintillation detectors, to other types of detectors where reactions induced by fast neutrons on carbon require an accurate description.

© 2017 Elsevier B.V. All rights reserved.

1. Introduction

Organic scintillation detectors are a standard choice in fast neutron detection and spectrometry for their high intrinsic detection efficiency over a wide energy range, fast response and, in some cases, good n–γ discrimination capabilities [1]. The accurate determination of their neutron response – as an essential part of their experimental characterization – is difficult and expensive, since it demands well calibrated sources of monoenergetic neutrons available only in a few metrology facilities and nuclear physics laboratories. A number of Monte Carlo simulation tools currently available have reached a high level of versatility and reliability that can be exploited to minimize the effort and cost implied, especially for complex detection systems for which the experimental characterization is more challenging.

NRESP is a Monte Carlo simulation code developed at the Physikalisch-Technische Bundesanstalt (PTB), Germany, to study the response of organic scintillation detectors to fast neutrons between 0.02 and 20 MeV [2]. It has been successful in describing the experimental

response functions of BC501A and NE213 detectors to monoenergetic neutrons with an uncertainty lower than 2% [3], and can be considered a state-of-the-art code in its application field. However, it cannot be used to simulate complex experiments and detection systems where a detailed geometric modeling and the transport of particles other than neutrons are required.

The GEANT4 simulation toolkit [4] is a more versatile and flexible tool widely used by the Nuclear and High Energy Physics scientific communities. Several authors have reported on its excellent accuracy in the calculation of the neutron response function of organic scintillation detectors below $E_n = 6$ MeV, where neutron scattering is the dominant reaction mechanism [5–7]. At higher energies, however, a significant underestimation of the experimental response function in the low pulse height range has been observed. Such discrepancies are a consequence of the incompleteness of the neutron interaction models and the evaluated nuclear data in GEANT4. Indeed, a close look into the implementation of the high precision model *G4ParticleHP* reveals that

the important ^{12}C(n,n'3α) reactions are not described properly when considered as multistep breakup reactions involving an intermediate nucleus in an excited state. Moreover, it lacks angular distribution data for the ^{12}C(n,α)^{9}Be reaction occurring above 6.18 MeV, which makes a significant contribution to the low pulse height range of the neutron response function.

This work aims at providing GEANT4 with the necessary models and data for a complete description of neutron-induced alpha production reactions on carbon as they are considered in NRESP. The results have been verified against simulations with NRESP and validated against Time-Of-Flight (TOF) measurements with an NE213 scintillation detector in quasi-monoenergetic neutron reference fields at PTB. The effects of using different standard evaluated nuclear data libraries have also been investigated.

2. Complete description of the ^{12}C(n,n'3α) and ^{12}C(n,α)^{9}Be reactions in GEANT4

G4ParticleHP[1] can be considered the best model in GEANT4 for the simulation of neutron interactions up to 20 MeV, as it employs evaluated nuclear data. Some reactions, however, are only partially described or not described at all by this model, either because of incomplete or missing information in the data libraries, or an incomplete implementation of the model itself. The latter is the case of breakup reactions proceeding in multiple steps, e.g., ^{12}C(n,n'3α).

The base class *G4ParticleHPInelasticBaseFS* and its derived classes in *G4ParticleHP* are devoted to describing reactions that involve more than one particle and a residual nucleus in the final state. These classes use, when available, evaluated energy–angle distributions to sample the final state of the reaction products, otherwise, the n-body phase space distribution. Reactions involving only one particle and a residual nucleus in the final state are described in *G4ParticleHPInelasticCompFS* and its derived classes instead. The description is however incomplete when it comes to breakup reactions proceeding in multiple steps, as they are not considered to their whole extent but only to the first step, leaving an intermediate nucleus in an excited state that is forced to decay to the ground state without any particle emission.

G4ParticleHPInelasticCompFS has been modified to incorporate the ^{12}C(n,n'3α) multistep breakup model from NRESP7.1 [2]. Two different mechanisms are considered in the model:

(I) $n + {}^{12}C \rightarrow \alpha + {}^9Be^* \mid {}^9Be^* \rightarrow n' + {}^8Be \mid {}^8Be \rightarrow 2\alpha$
(II) $n + {}^{12}C \rightarrow n' + {}^{12}C^* \mid {}^{12}C^* \rightarrow \alpha + {}^8Be \mid {}^8Be \rightarrow 2\alpha$.

Both end up with the 2α decay of ^{8}Be from its ground state but differ in the initial and intermediate steps. Each mechanism comprises one or more reaction channels associated with excited well-defined states or pseudo-states of the intermediate nucleus (Table 1). The model samples the direction of the outgoing neutron from an isotropic distribution in the center-of-mass system and the alpha particles are emitted conserving energy and momentum. Relativistic kinematics is applied at each step.

Even using the same physics models, one can expect different results when simulating the neutron response of organic scintillation detectors with GEANT4 and NRESP due to differences in the nuclear data. *G4ParticleHP* relies on the evaluated neutron data library G4NDL distributed with GEANT4. Version 4.5 of G4NDL, which was used in this work, is based on ENDF/B-VII.1 [13]. NRESP7.1, on the other hand, takes nuclear data for hydrogen from ENDF/B-IV [14], and for carbon and aluminum from ENDF/B-VI [8,9]. Itscross section data on neutron-induced reactions on carbon were initially taken from ENDF/B-VI and have been partially replaced over time by data from dedicated experiments performed at PTB, readjusting the balance with other reactions to keep the total cross section – which is a well known quantity – unchanged.
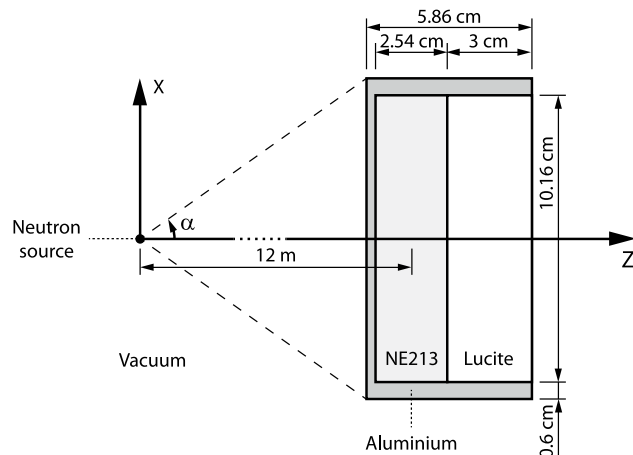

Fig. 1. Geometrical aspects of the simulations. They reproduce the relevant features of the Time-Of-Flight measurements presented in Section 4.

Differences in the cross section data affect the contribution of the corresponding reactions to the neutron response function. The effect for angular distributions is somewhat more complex, because they determine the energy distributions of the reaction products and, as it will be shown in the next section, the light produced by charged particles in an organic scintillator depends on the particle type and kinetic energy. Hence, uncertainties in the angular distributions propagate to the light yield affecting the shape of the response function.

G4NDL-4.5 has angular distribution data for some of the ^{12}C(n,n'3α) reactions. These are ignored by the multistep breakup model. The ^{12}C(n,α)^{9}Be reaction, on the other hand, has a strong anisotropy in the center-of-mass system that is considered by NRESP but neglected in G4NDL-4.5. This reaction contributes to the same pulse height range of the neutron response function as the ^{12}C(n,n'3α) reactions. For this reason, in addition to the multistep breakup model for the ^{12}C(n,n'3α) reactions, the angular distribution data for the ^{12}C(n,α)^{9}Be reaction in NRESP7.1 were also incorporated (hard coded) into *G4ParticleHPInelasticCompFS*. The result of all modifications made to *G4ParticleHPInelasticCompFS* is a complete description in GEANT4 of neutron-induced alpha production reactions on carbon.

3. Verification against NRESP

3.1. Simulations

Simulations with the standard (official distribution) and modified (resulting from this work) versions of GEANT4 (release 10.02.p02) were performed to calculate the neutron response function of an NE213[2] detector. Equivalent simulations were also performed with NRESP7.1 to verify the results.

The detector simulated was a simplified model of the one used in the Time-Of-Flight measurements that will be presented in the next section. It consisted of a $4'' \times 1''$ NE213 cylindrical volume coupled to a Lucite light pipe, both enclosed by an aluminum housing as shown in Fig. 1. To meet the limitations of NRESP in material chemical compositions, the small amounts of oxygen and other chemical elements present in NE213 ($\leq$1%) were neglected, and the oxygen in Lucite ($C_5H_8O_2$) was replaced with carbon with the corresponding density readjustment. Both materials were thus considered pure hydrocarbons with H:C atom ratios 1.213 and 1.1, and densities 0.8752 and 1.18 g/cm^3, respectively.

The neutron response function was calculated for energies between 6.18 MeV (threshold of the ^{12}C(n,α)^{9}Be reaction) and 20 MeV (upper applicability limit of the *G4ParticleHP* model for neutrons). A total of

Table 1
Neutron-induced reactions on carbon between 0 and 20 MeV in NRESP7.1 [2]. The lowest excited states of ^{12}C denoted by L1, L2 and L3 are well-defined states. The rest (L6 to L10) are pseudo-states that represent groups of well-defined states at higher excitation energies.

Reaction	Q_I (MeV)[*]	Threshold (MeV)	Cross section	Angular distribution
^{12}C(n,n)^{12}C	0	0	ENDF/B-VI [8,9]	ENDF/B-VI [8]
^{12}C(n,n′)^{12}C*(L1)	−4.439	4.81	ENDF/B-VI [8,9]	ENDF/B-VI [8,9]
^{12}C(n,α)^{9}Be	−5.71	6.19	PTB [10,11]	PTB [10,11]
^{12}C(n,α)^{9}Be* → n + ^{8}Be → 2α	−8.13	8.81	PTB	Isotropic[**]
^{12}C(n,n′)^{12}C*(L2) →α + ^{8}Be → 2α	−7.653	8.29	PTB	Isotropic[**]
^{12}C(n,n′)^{12}C*(L3) →α + ^{8}Be → 2α	−9.63	10.43	PTB	Isotropic[**]
^{12}C(n,n′)^{12}C*(L4) →α + ^{8}Be → 2α	−10.8	11.70	PTB	Isotropic[**]
^{12}C(n,n′)^{12}C*(L5) →α + ^{8}Be → 2α	−11.8	12.78	PTB	Isotropic[**]
^{12}C(n,n′)^{12}C*(L6) →α + ^{8}Be → 2α	−12.7	13.76	PTB	Isotropic[**]
^{12}C(n,n′)^{12}C*(L7) →α + ^{8}Be → 2α	−14	15.17	PTB	Isotropic[**]
^{12}C(n,n′)^{12}C*(L8) →α + ^{8}Be → 2α	−15	16.25	PTB	Isotropic[**]
^{12}C(n,n′)^{12}C*(L9) →α + ^{8}Be → 2α	−16	17.33	PTB	Isotropic[**]
^{12}C(n,n′)^{12}C*(L10) →α + ^{8}Be → 2α	−17	18.42	PTB	Isotropic[**]
^{12}C(n,p)^{12}B	−12.59	13.7	ENDF/B-VI [8,9]	Isotropic[**]
^{12}C(n,d)^{11}B	−13.731	14.9	ENDF/B-VI [8,9]	Isotropic[**]

[*] Q-value for the energy state of the residual nucleus (intermediate nucleus for multistep breakup reactions) [12].

[**] Referred to the center-of-mass system.

10^7 neutrons were generated for each energy from a point source 12 m away from the center of the scintillation volume of the detector (Fig. 1). The generation was isotropic and only within the solid angle subtended by the detector to reduce the computation time.

GEANT4 allows for a more detailed particle transportation than NRESP. In this sense, it can be considered more realistic but also more time-consuming. Neutrons in GEANT4 were transported in vacuum from the source to the detector housing, and tracked until they were captured or escaped the detector. All secondary particles giving rise to fluorescent light in the scintillator [15] were also tracked, and the light yield was calculated at the end of each step. NRESP, on the other hand, stops the transportation of neutrons when the kinetic energy is below 10 keV. It does not transport secondary particles, but assumes instead that all their energy is deposited at the generation point, where part of it is then converted into fluorescent light. The only exceptions regarding the energy deposition are protons and gamma rays. The energy deposited by recoil protons generated in the scintillator is corrected to account for the wall effects when the range is longer than the distance to the scintillator surface. In the case of gamma rays, the energy deposition is considered only for those produced in the ^{12}C(n,n′γ)^{12}C reaction. This is done in a very schematic way when the light yield resulting from other reactions initiated by the same incident neutron exceeds a certain threshold. When it does not, the detection event is discarded, as it is assumed that it would also be discarded with the application of n–γ discrimination techniques in the experimental determination of the response function. In the present work, the contribution of gamma rays to the detector response was neglected in the simulations with both GEANT4 and NRESP, because it is not relevant for the verification of the modified version of the former against the latter, nor it is for the validation against TOF measurements presented in the next section.

The production and tracking of secondary particles in GEANT4 are determined by the physics models. The production is also affected by the production cuts, which are thresholds in stopping range. A few standard physics lists are distributed with GEANT4 for different applications, featuring different combinations of these. We have used *Shielding* in this work [16], which features the *Standard Electromagnetic* and *G4ParticleHP* models. The rest of the standard physics lists featuring the same hadronic models were verified to produce equivalent results with the same production cuts.

The production cut for protons and heavier ions in *Shielding* is set to 0 mm by default. This is essential for the simulation of organic scintillation detectors, because it ensures that recoil ions are always produced regardless of the amount of energy transferred by the neutron. The production of delta electrons, on the contrary, must be suppressed, because their contribution to the light yield of protons and heavier ions is already included in the light output functions of the latter. The default
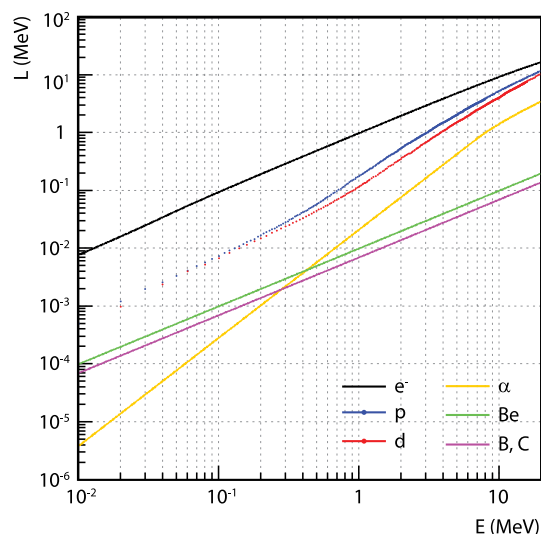

Fig. 2. Light output functions for secondary charged particles produced in the interaction of neutrons with a $4'' \times 1''$ NE213 scintillation detector.

production cut of 0.7 mm was enough to suppress the delta electron production.

Fig. 2 shows the light yield of different charged particles for a detector of the same type and dimensions than the one considered in this work. These functions were selected from the wide set available in the data files of NRESP7.1.

The light output function for electrons is described by $L_e = E - 0.005$ MeV above 50 keV [17]. The offset approximates the non-linear dependence at lower energies, which is an effect of quenching processes [15]. For protons and heavier ions, the light output functions are:

$$L_p(E_p) = -1.41945 + 0.6719E_p \qquad E_p \geq 8 \text{ MeV}$$
$$L_d(E_d) = 2L_p(0.5E_d)$$
$$L_\alpha(E_\alpha) = \begin{cases} 0.0211E_\alpha^{1.8712} & E_\alpha < 6.76 \text{ MeV} \\ -0.65665 + 0.20864E_\alpha & E_\alpha \geq 6.76 \text{ MeV} \end{cases}$$
$$L_{Be}(E_{Be}) = 0.01E_{Be}$$
$$L_{B,C}(E_{B,C}) = 0.007E_{B,C}$$

Only for protons with $E_p < 8$ MeV, the light yield is calculated by linear interpolation of a set of discrete experimental values [3].

3.2. Results and discussion

Fig. 3 shows the neutron response functions $R(L)$ calculated with NRESP and the standard and modified versions of GEANT4. They –
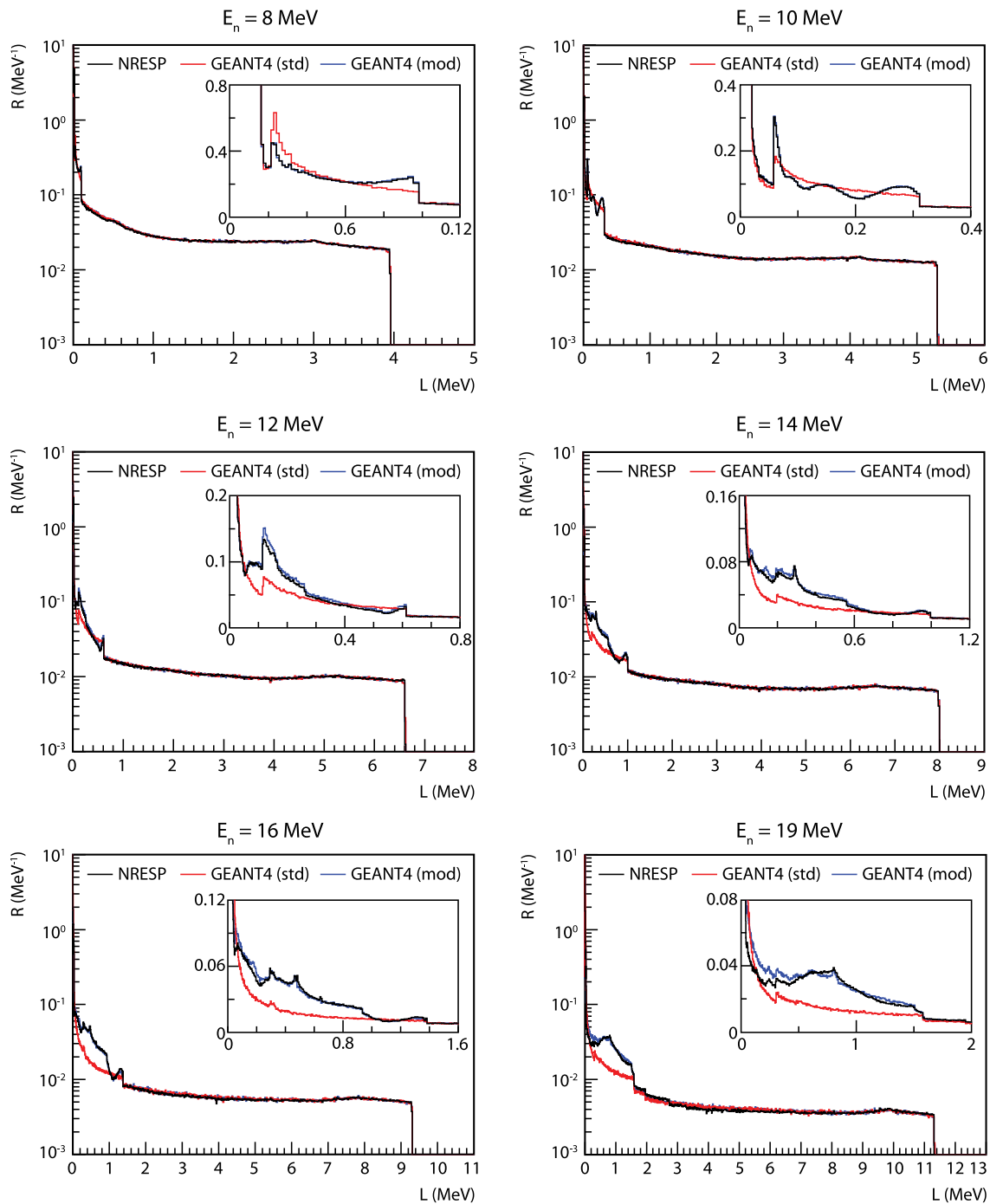
Fig. 3. Neutron response functions calculated with NRESP and the standard (std) and modified (mod) versions of GEANT4. The amount of scintillation light L produced by secondary charged particles is given in electron equivalent units.

and any other presented hereafter – are the pulse height distribution of detected neutrons in electron equivalent units (i.e., the kinetic energy of an electron producing the same amount of light) normalized to the total intrinsic detection efficiency. In other words, the content of each bin is the result of scaling the distribution by the inverse of the number of neutrons incident on the detector and the bin width. The figure also shows embedded zooms into the low pulse height range for a better visualization of the contributions of the $^{12}C(n,\alpha)^9Be$ and $^{12}C(n,n'3\alpha)$ reactions.

All simulations are in excellent agreement in the mid and high pulse height ranges, where proton recoil events dominate. It is in the low range where discrepancies due to the different description of neutron-induced reactions on carbon are observed, illustrating the importance

of a complete and accurate description of these reactions in the study of the neutron response of organic scintillation detectors.

The correct incorporation of angular distributions for the $^{12}C(n,\alpha)^9Be$ reaction into GEANT4 can be verified by comparing the response functions calculated with the modified version of GEANT4 and NRESP for neutron energies below the threshold of the $^{12}C(n,n'3\alpha)$ reactions (8.81 MeV). The agreement is excellent for 8 MeV, and also for 10 MeV where the $^{12}C(n,n'3\alpha)$ reactions make a negligible contribution. At higher energies, the combined effect with the incorporation of the multistep breakup model for the $^{12}C(n,n'3\alpha)$ reactions is observed instead. NRESP and the modified version of GEANT4 continue to be in an excellent agreement that slightly worsens with the increase of the neutron energy due to differences in the cross section data.
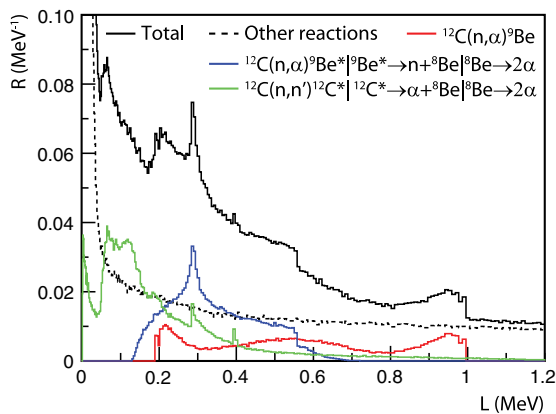
Fig. 4. Partial contributions to the neutron response function of the neutron-induced alpha production reactions on carbon, calculated with the modified version of GEANT4 for 14 MeV neutrons. The amount of scintillation light L produced by secondary charged particles is given in electron equivalent units.

Fig. 4 helps to understand the structures observed in the low pulse height range of the neutron response functions. It shows the partial contributions of the $^{12}C(n,\alpha)^9Be$ and $^{12}C(n,n'3\alpha)$ reactions to the neutron response function calculated with the modified version of GEANT4 for 14 MeV neutrons. The $^{12}C(n,\alpha)^9Be$ reaction produces a regular structure with high and low endpoints corresponding to the forward and backward emission of the alpha particle respectively, with respect to the direction of the incident neutron. The contributions of the $^{12}C(n,n'3\alpha)$ reactions are somewhat more complex because of the different mechanisms, multiple steps and number of excited states of the intermediate nucleus involved. The net effect of these reactions on the neutron response function is determined by the cross section and angular distribution data.

3.3. Nuclear data library effects on the neutron response function

The International Atomic Energy Agency (IAEA) Nuclear Data Service distributes different versions of standard nuclear data libraries for GEANT4 [18] produced by E. Mendoza et al. [19,20] at Centro de Investigaciones Energéticas, Medioambientales y Tecnológicas (CIEMAT), Spain. We have chosen ENDF/B-VII.1 [13], JEFF-3.2 [21], JENDL-4.0 [22] and CENDL-3.1 [23,24] in addition to G4NDL-4.5, for investigating the effects of using different nuclear data libraries in the study of the neutron response of organic scintillation detectors. JEFF-3.2 takes the data on neutron-induced reactions on carbon from ENDF/B-VII.1, which was used to produce G4NDL-4.5. We have verified that GEANT4 produces the same results with these three libraries. Thus, the results presented here for G4NDL-4.5 are representative of ENDF/B-VII.1 and JEFF-3.2.

The neutron response functions calculated with the modified version of GEANT4 using G4NDL-4.5, JENDL-4.0 and CENDL-3.1 are compared in Fig. 5. Only the low pulse height range is shown, since the agreement is excellent in the mid and high ranges where proton recoil events dominate. The response functions calculated using G4NDL-4.5 and JENDL-4.0 show discrepancies that result from the differences in the cross section data on the $^{12}C(n,\alpha)^9Be$ and $^{12}C(n,n'3\alpha)$ reactions (Fig. 6), and also from the different number of excited states of ^{12}C considered in each library. Data on the $^{12}C(n,n'3\alpha)$ reactions in G4NDL-4.5 and JENDL-4.0 are only available for the multistep breakup model, with more than twice the number of excited states of ^{12}C in JENDL-4.0[3]. CENDL-3.1, on the other hand, has data on the second and third

excited states of ^{12}C for the multistep breakup model, and energy–angle distributions to describe the rest of the $^{12}C(n,n'3\alpha)$ reactions [12]. Thus, discrepancies with the response functions calculated using CENDL-3.1 result also from the use of a different model.

Fig. 5 also shows the neutron response functions calculated with the standard version of GEANT4 using CENDL-3.1. These already show structures that result from sampling the final state of the $^{12}C(n,n'3\alpha)$ reactions from energy–angle distributions. However, they do not resemble the neutron response functions calculated with the modified version of GEANT4 using the other libraries. The reason lies in the lack of correlation between reaction products of the $^{12}C(n,n'3\alpha)$ reactions in CENDL-3.1. As a result, the energy is not conserved in an event-by-event basis but only statistically, broadening out narrow structures.

Table 2 presents the deviations relative to NRESP, of the intrinsic neutron detection efficiencies calculated with GEANT4. They were calculated for different detection thresholds with the standard and modified versions of GEANT4 using different nuclear data libraries. The decreasing trend in the magnitude of the deviations with the increase of the threshold in most cases confirms that the discrepancies between the response functions are mainly in the low pulse height range. On the contrary, there is an increasing trend with the increase of the neutron energy as those discrepancies are enhanced, becoming as large as 23% with the standard version of GEANT4 using JENDL-4.0.

The largest in magnitude of the deviations calculated with the standard version of GEANT4 using CENDL-3.1 is much lower (<5%) as expected. It is surprising though that these are systematically higher when the modified version of GEANT4 is used instead. In any case, this is not an indication of a good agreement with NRESP, but a compensation effect of opposite deviations in contiguous pulse height ranges that partially cancel out when integrating the response function to calculate the detection efficiency.

A comparison between the response functions and deviations calculated with the different versions of GEANT4 reveals a similar effect for G4NDL-4.5 and JENDL-4.0 at 8 and 10 MeV, where the discrepancies between the response functions are dominated by the $^{12}C(n,\alpha)^9Be$ reaction. At higher neutron energies (14–19 MeV), the deviations are significantly reduced in magnitude with the modified version of GEANT4 as the $^{12}C(n,n'3\alpha)$ reactions become more relevant.

In average, the best agreement with NRESP is obtained with the modified version of GEANT4 using G4NDL-4.5.

4. Validation against Time-Of-Flight measurements

4.1. Description of the experiment

Time-Of-Flight (TOF) measurements were performed at the PTB Ion Accelerator Facility (PIAF) to validate the modified version of GEANT4 and draw conclusions on its performance with different standard evaluated nuclear data libraries. An NE213 detector like the one described in the previous section (Fig. 1) was used to provide the start signal for the determination of the TOF. It was placed 12 m from the target at 0°with respect to the direction of the beam. This is a well characterized detector that has been used for many years as a reference instrument for the measurement of the neutron fluence at the PTB TOF spectrometer.

The neutron fields were produced by inducing the $D(d,n)^3He$ reaction in a 3 cm thick gas target at a pressure of 1.8 bar. The reaction produced quasi-monoenergetic neutrons based upon the incident deuteron energy, and a continuum of unwanted low-energy neutrons from the D(d,np)D and D(d,np)np reactions. In addition to these, a continuum of neutrons was also produced from the reactions of incident deuterons in the backing of the target (the typical energy loss in the target is ≤100 keV).

The deuteron beams were delivered by the variable energy isochronous cyclotron CV28 [25] at a repetition frequency reduced to about 1 MHz with the internal beam pulse selector. Most unwanted pulses were suppressed with an efficiency of 98%. The contribution
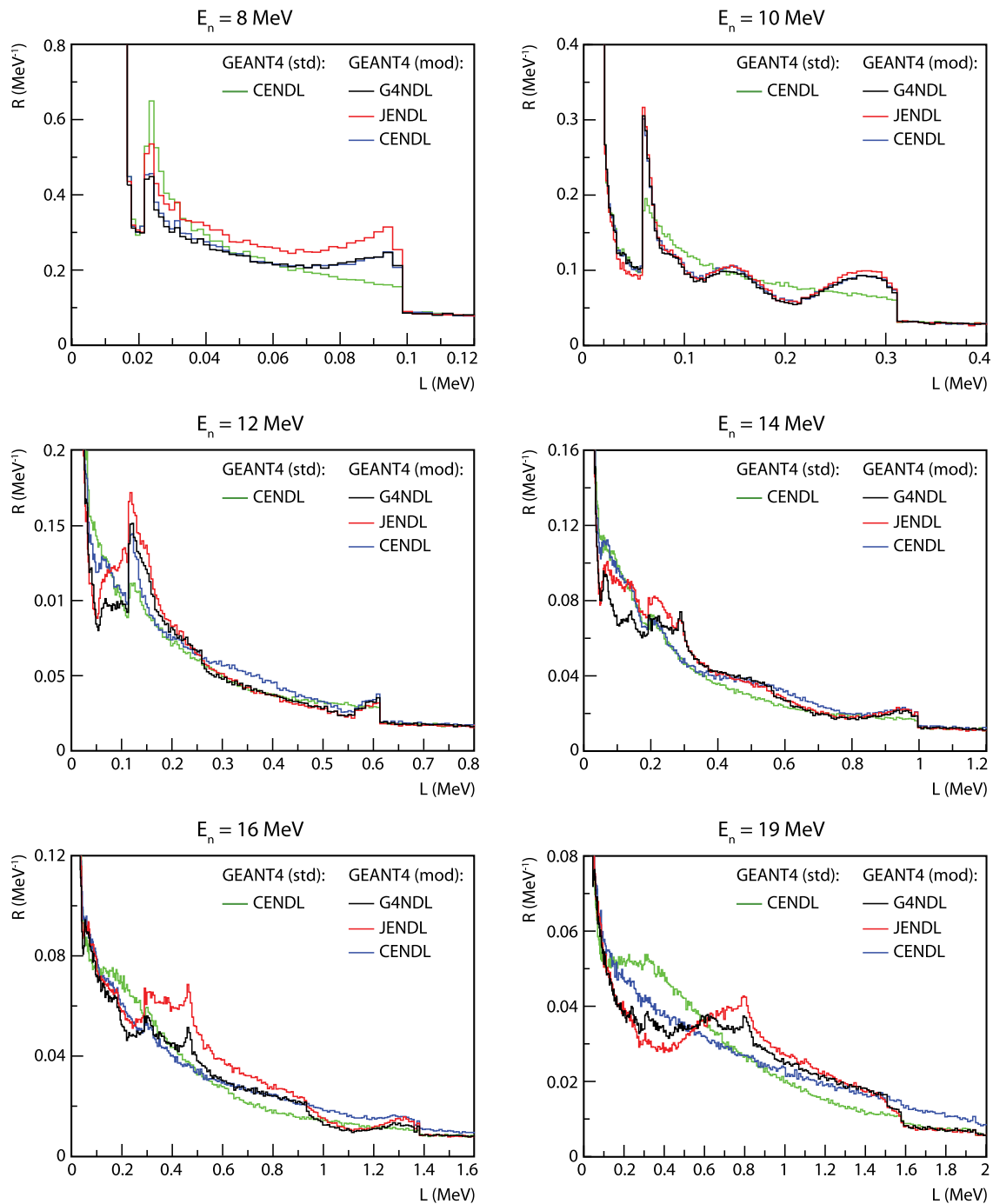
---

[3] Carbon data in ENDF/B-VII.1, JEFF-3.2 and JENDL-4.0 are actually given for natural carbon. We use throughout the text the most abundant isotope ^{12}C instead, to unify the nomenclature with CENDL-3.1, which does contain data for this specific isotope.

Fig. 5. Low pulse height range of the neutron response functions of a $4'' \times 1''$ NE213 detector calculated with the standard (std) and modified (mod) versions of GEANT4 using different evaluated nuclear data libraries. The amount of scintillation light L produced by secondary charged particles is given in electron equivalent units.

of the rest was corrected in the TOF versus pulse height matrices using an iterative subtraction procedure. The stop signal for the TOF measurements was derived from the deuteron beam pulses using an inductive pick-up close to the gas target.

A multiparameter data acquisition system based on NIM and VME modules was used to process the signals from the detector and the cyclotron, and derive with these the TOF spectra. The pulse height spectra were obtained by setting adequate windows on the TOF spectra around the peak of quasi-monoenergetic neutrons from the $\mathrm{D}(d,n)^3\mathrm{He}$ reaction, and removing the contributions unwanted events. To determine the contribution of neutrons from the deuteron reactions in the backing of the target, measurements without gas in the target (gas-out) were also performed. The difference with measurements with gas in the

target (gas-in) still contained a contribution of gamma rays that was removed by pulse shape analysis. Corrections for satellites pulses, events randomly distributed over the time scale and dead time losses were also performed.

More information about standard TOF measurements at PTB can be found in [26–28]. See also [25] for a detailed description of the facility.

4.2. Results and discussion

Fig. 7 shows the measured neutron response functions compared with the response functions calculated with the modified version of GEANT4 using G4NDL-4.5 and CENDL-3.1. The resolution of the detection system was taken into account in the latter by folding with a

Table 2
Relative deviations $\Delta_{GEANT4} = (\varepsilon_{GEANT4} - \varepsilon_{NRESP})/\varepsilon_{NRESP}$ with respect to NRESP, of the intrinsic neutron detection efficiency calculated with the standard (std) and modified (mod) versions of GEANT4. The relative statistical uncertainties are <0.03%. The thresholds are indicated in electron equivalent units.

| E_n (MeV)	Threshold (MeV)	ε_{NRESP} (%)	Δ_{GEANT4}^{std} (%)			Δ_{GEANT4}^{mod} (%)		
			G4NDL-4.5	JENDL-4.0	CENDL-3.1	G4NDL-4.5	JENDL-4.0	CENDL-3.1
	0.12	10.65	1.49	0.50	1.89	1.55	0.58	2.10
8	0.16	10.38	1.39	0.43	1.79	1.45	0.52	2.03
	0.2	10.10	1.26	0.37	1.71	1.31	0.47	1.93
	0.12	9.48	0.98	0.83	1.16	1.09	1.33	1.67
10	0.16	9.13	0.81	0.45	0.91	1.07	1.11	1.47
	0.2	8.82	0.28	−0.37	0.33	1.02	0.83	1.30
	0.12	8.94	−3.58	−4.30	1.20	2.65	3.02	3.87
12	0.16	8.49	−1.58	−2.49	2.09	2.24	2.00	4.21
	0.2	8.11	−0.10	−1.16	2.55	2.09	1.48	4.68
	0.12	8.38	−10.32	−9.38	−0.71	3.03	4.39	3.34
14	0.16	8.14	−9.40	−8.57	−1.74	2.80	3.40	2.35
	0.2	7.89	−8.28	−7.57	−2.43	2.60	2.61	1.87
	0.12	8.19	−18.20	−15.73	0.87	1.19	9.14	4.00
16	0.16	7.95	−17.61	−15.25	0.38	1.10	9.14	3.76
	0.2	7.72	−16.97	−14.71	−0.67	0.70	8.81	3.16
	0.12	7.92	−20.43	−22.64	4.54	4.23	5.21	6.89
19	0.16	7.78	−20.76	−23.04	3.84	3.82	4.78	6.16
	0.2	7.65	−20.97	−23.34	2.75	3.38	4.32	5.30
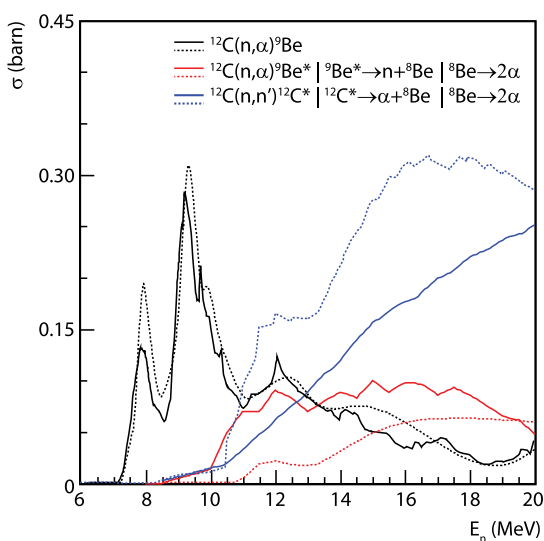
Fig. 6. Cross sections of neutron-induced alpha production reactions on carbon in G4NDL-4.5 (continuous line) and JENDL-4.0 (dotted line). G4NDL-4.5 is representative of ENDF/B-VII.1 and JEFF-3.2.

Gaussian distribution of full width at half maximum (ΔL) given by the resolution function:

$$\frac{\Delta L}{L} = \sqrt{\alpha + \frac{\beta}{L} + \frac{\gamma}{L^2}}$$

Parameters $\alpha = 7.569 \cdot 10^{-3}$, $\beta = 9.409 \cdot 10^{-3}$ MeV and $\gamma = 2.5 \cdot 10^{-5}$ MeV^2 were determined from calibration measurements with standard gamma sources by the procedure described in [29].

The agreement between simulations and experiment is excellent in the mid and high pulse height ranges. In the low range, conclusions can only be drawn at 10.11, 12.11 and 13.90 MeV, where, unlike at 8.11 MeV, the contribution of the $^{12}C(n,\alpha)^9Be$ and $^{12}C(n,n'3\alpha)$ reactions extend above the experimental detection threshold. The simulations describe well the contributions of these reactions in gross terms, but it is with G4NDL-4.5 that the structures – now smoothed by the resolution of the detector system – are best reproduced.

Table 3 presents the deviations relative to the experiment, of the intrinsic neutron detection efficiencies calculated with NRESP and the standard and modified versions of GEANT4. The efficiencies were calculated with an experimental detection threshold corresponding to

an electron equivalent energy of 0.16 MeV. What stands out in the table at first glance is the significant reduction in magnitude of the deviations calculated with GEANT4 when the modified version is used. This happens for all three libraries and at all neutron energies except the lowest, where there is no difference whatsoever for the reasons aforementioned. It also stands out from the table that, at 12.11 MeV, both the modified version of GEANT4 and NRESP produce deviations significantly larger in magnitude than at other energies. Possible explanations may be found in the experiment (e.g., a contribution of gamma rays that the pulse shape discrimination failed to remove), but in general, the quality of the nuclear data and light functions, and the approximations in the models, are the major responsibles for the differences that persist between the simulated and experimental response functions (see the zooms in Fig. 7).

Contrary to the conclusions drawn in Section 3.3, relative to the experiment, the modified version of GEANT4 produces deviations lower in magnitude than the standard version when used with CENDL-3.1. They are even lower than the ones obtained with the modified version of GEANT4 using G4NDL-4.5, but this is again a compensation effect and not an indication of a better agreement with the experiment. The effect can be observed best in the zooms into the low pulse height range in Fig. 7 at 12.11 and 13.90 MeV. Between the experimental threshold up to approximately 0.4 MeV, the modified version of GEANT4 used with CENDL-3.1 underestimates the experimental response. An overestimation of about the same magnitude is observed instead at higher energies, which reduces as the contribution of the $^{12}C(n,\alpha)^9Be$ and $^{12}C(n,n'3\alpha)$ reactions decreases.

5. Conclusions

The capacity of GEANT4 to study the neutron response of organic scintillation detectors in the energy range from 0 to 20 MeV has been substantially improved by providing it with a complete description of neutron-induced alpha production reactions on carbon. We have modified the high precision model *G4ParticleHP* to incorporate, from NRESP7.1, the multistep breakup model for the $^{12}C(n,n'3\alpha)$ reactions and missing angular distribution data for the $^{12}C(n,\alpha)^9Be$. The results have been verified against simulations with NRESP and validated against Time-Of-Flight measurements performed at PTB.

The largest deviations of the intrinsic neutron detection efficiency relative to NRESP were reduced from 20% to 5% in magnitude. With respect to the experiment, the reduction was from 12% to 6%. Further improvements can be achieved with better cross section and angular distribution data, as well as more accurate light output functions for the detector in question.
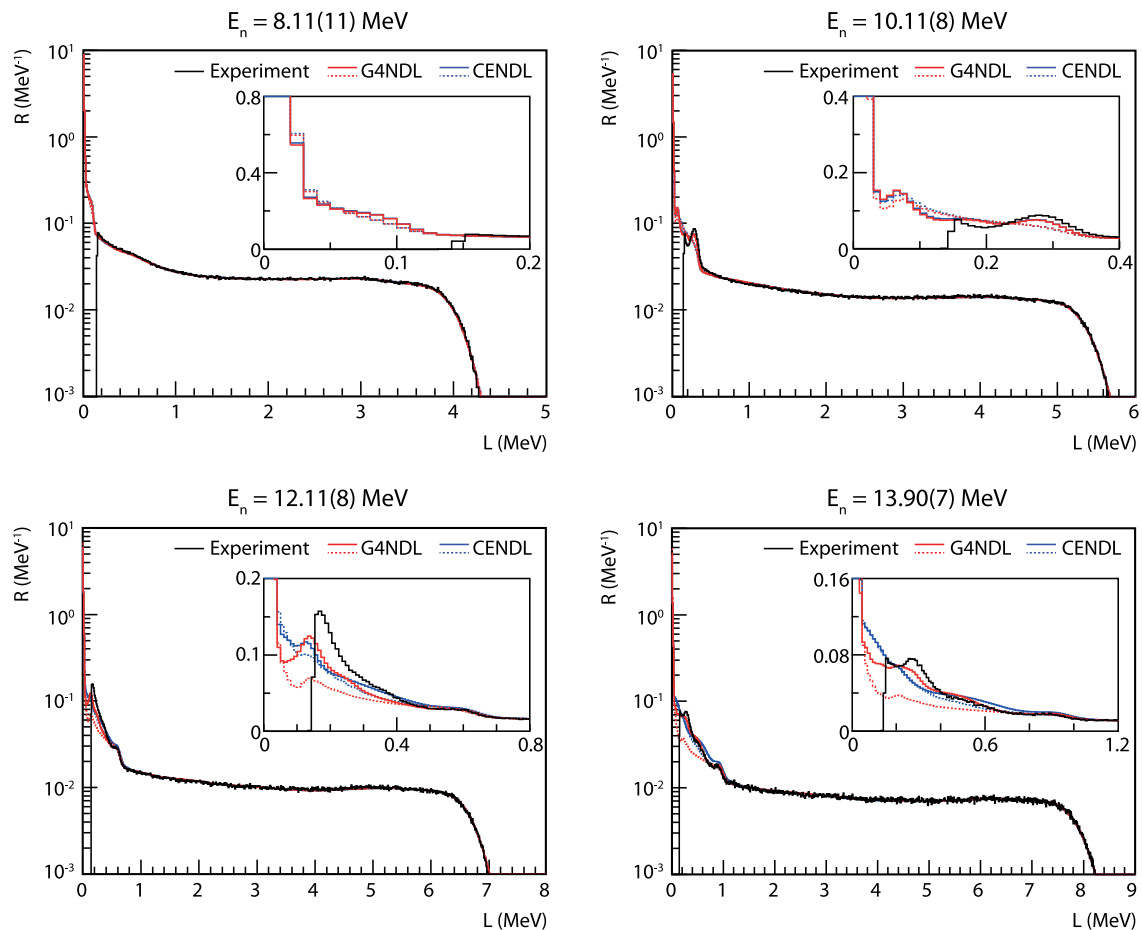
Fig. 7. Neutron response functions of a $4'' \times 1''$ NE213 detector from Time-Of-Flight measurements and calculations with the standard (dotted line) and modified (continuous line) versions of GEANT4. The amount of scintillation light L produced by secondary charged particles is given in electron equivalent units.

Table 3
Relative deviations $\Delta = (\varepsilon - \varepsilon_{\exp})/\varepsilon_{\exp}$ with respect to the Time-Of-Flight measurements performed at PTB (exp), of the intrinsic neutron detection efficiency calculated with NRESP and the standard (std) and modified (mod) versions of GEANT4. Efficiencies from Monte Carlo simulations were calculated with a relative statistical uncertainty <0.01%. The uncertainty in the experimental efficiencies are standard measurement uncertainties for a coverage factor $k = 1$. All efficiencies were calculated with a threshold corresponding to an electron equivalent energy of 160 keV.

E_n (MeV)	$\varepsilon_{\exp}$ (%)	Δ_{NRESP} (%)	$\Delta_{\mathrm{GEANT4}}^{\mathrm{std}}$ (%)			$\Delta_{\mathrm{GEANT4}}^{\mathrm{mod}}$ (%)		
			G4NDL-4.5	JENDL-4.0	CENDL-3.1	G4NDL-4.5	JENDL-4.0	CENDL-3.1
8.11(11)	10.6(3)	−1.6(5)	−1.6(5)	−2.0(6)	−0.9(3)	−1.6(5)	−2.1(7)	−0.9(3)
10.11(8)	9.3(2)	−1.2(2)	−2.1(4)	−1.9(4)	−1.9(4)	−1.1(2)	−0.58(11)	−0.79(15)
12.11(8)	9.4(2)	−7.5(14)	−11(2)	−12(2)	−7.3(14)	−6.2(12)	−7.1(13)	−4.9(9)
13.90(7)	8.4(2)	−2.5(4)	−12(2)	−12(2)	−5.1(9)	−1.4(2)	−0.6(1)	−1.0(2)

The effect on the neutron response function of using different evaluated nuclear data libraries (G4NDL-4.5, ENDF/B-VII.1, JEFF-3.2, JENDL-4.0 and CENDL-3.1) was also investigated. The relative deviations of the intrinsic neutron detection efficiency from the experiment did not allow to conclude which library the modified version of GEANT4 (resulting from this work) performs best with. Whereas the experimental response function was better reproduced with libraries where the ^{12}C(n,n′3α) reactions are considered to undergo a multistep breakup (G4NDL-4.5, ENDF/B-VII.1, JEFF-3.2, JENDL-4.0), the deviations lowest in magnitude were obtained with CENDL-3.1, which contains energy–angle distributions for most of them instead.

G4ParticleHP could already sample the final state of breakup reactions from energy–angle distributions. In consequence, the standard version of GEANT4 (official release) produced better results with CENDL-3.1 than with any other library. Even in this case, the results were further improved with the modified version of GEANT4, with the description of the rest of the ^{12}C(n,n′3α) reactions considered to undergo a multistep breakup that were omitted before.

This work has potential applications beyond organic scintillation detectors, to other types of detectors where reactions induced by fast neutrons on carbon require an accurate description, e.g., diamond detectors [30] and Tissue-Equivalent Proportional Counters (TEPC) [31]. All modifications to the *G4ParticleHP* model will be included in the forthcoming releases of GEANT4.

Acknowledgments

References

[1] H. Klein, F.D. Brooks, Scintillation detectors for fast neutrons, in: Proc. Int. Work. Fast Neutron Detect. Appl. Cape Town, South Africa, 2006.

[2] G. Dietze, H. Klein, NRESP4 and NEFF4: Monte Carlo codes for the calculation of neutron response functions and detection efficiencies for NE213 scintillation detectors, Physikalisch-Technische Bundesanstalt (PTB), PTB-ND-22, Braunschweig, Germany, 1982.

[3] D. Schmidt, et al., Characterization of liquid scintillation detectors, Nucl. Instrum. Methods A 476 (2002) 186–189.

[4] S. Agostinelli, et al., Geant4 — a simulation toolkit, Nucl. Instrum. Methods A 506 (2003) 250–303.

[5] N. Patronis, et al., Aspects of GEANT4 Monte-Carlo calculations of the BC501A neutron detector, Nucl. Instrum. Methods A 578 (2007) 351–355.

[6] M. Gohil, et al., Measurement and simulation of neutron response function of organic liquid scintillator detector, Nucl. Instrum. Methods A 664 (2012) 304–309.

[7] Z.S. Hartwig, P. Gumplinger, Simulating response functions and pulse shape discrimination for organic scintillation detectors with GEANT4, Nucl. Instrum. Methods A 737 (2014) 155–162.

[8] P.F. Rose (Comp. and Ed.), ENDF/B-VI summary documentation, BNL-NCS-17541 (4th edition), Brookhaven National Laboratory, Upton, New York, USA, 1991.

[9] V. McLane, et al., ENDF/B-VI Summary Documentation Supplement. 1: ENDF/HE-VI Summary Documentation, fourth ed., Brookhaven National Laboratory, BNL-NCS-17541, Upton, New York, USA, 1996.

[10] D. Schmidt, et al., Investigation of the ^{9}Be$(\alpha, N)^{12}$C Reaction. I: Experimental Procedure and Uncertainties, Physikalisch-Technische Bundesanstalt (PTB), PTB-N-7, Braunschweig, Germany, 1992.

[11] D. Schmidt, et al., Investigation of the ^{9}Be$(\alpha, N)^{12}$C Reaction. II: Differential Cross Sections for E_α, Braunschweig, Germany 1992.

[12] Cross Sections Evaluation Working Group, ENDF-6 Formats Manual: Data Formats and Procedures for the Evaluated Nuclear Data Files ENDF/B-VI and ENDF/B-VII, BNL-90365-2009, Brookhaven National Laboratory, Upton, New York, USA, 2011.

[13] M.B. Chadwick, et al., ENDF/B-VII1 Nuclear data for science and technology: Cross sections, covariances, fission product yields and decay data, Nucl. Data Sheets 112 (2011) 2887–2996.

[14] D Garber (Ed.), ENDF/B Summary Documentation, BNL-NCS-17541, second ed., Brookhaven National Laboratory, Upton, New York, USA, 1975.

[15] J.B. Birks, The Theory and Practice of Scintillation Counting, Pergamon Press, Oxford, England, 1964.

[16] T. Koi, G. Folger, Shielding physics list: for shielding, underground and high energy applications. http://www.slac.stanford.edu/comp/physics/geant4/slac_physics_lists/shielding/shielding.html. (Accessed 30 January 2017).

[17] G. Dietze, Energy calibration of NE-213 scintillation counters by δ-rays, IEEE Trans. Nucl. Sci. 26 (1979) 398–402.

[18] E. Mendoza, D. Cano-Ott, New evaluated neutron cross section libraries for the GEANT4 code, http://www-nds.iaea.org/geant4. (Accessed 30 January 2017).

[19] E. Mendoza, et al., New evaluated neutron cross section libraries for the GEANT4 code, International Atomic Energy Agency (IAEA), INDC(NDS)-0612, Vienna, Austria, 2012.

[20] E. Mendoza, New standard evaluated neutron cross section libraries for the GEANT4 code and first verification, IEEE Trans. Nucl. Sci. 61 (2014) 2357–2364.

[21] JEFF-32 evaluated data library - Neutron data, https://www.oecd-nea.org/dbforms/data/eva/evatapes/jeff_32. (Accessed 30 January 2017).

[22] K. Shibata, et al., JENDL-4.0: A new library for nuclear science and engineering, J. Nucl. Sci. Technol. 48 (2011) 1–30.

[23] Z. Youxiang, et al., CENDL-3 — Chinese evaluated nuclear data library, version 3, J. Nucl. Sci. Technol. 39 (2002) 37–39.

[24] Z.G. Ge, et al., The updated version of chinese evaluated nuclear data library (cendl-31), J. Korean Phys. Soc. 59 (2011) 1052–1056.

[25] H.J. Brede, et al., The braunschweig accelerator facility for fast neutron research. 1: building design and accelerators, Nucl. Instrum. Methods 169 (1980) 349–358.

[26] D. Schmidt, H. Klein, Precise Time-of-Flight spectrometry of fast neutrons - Principles, methods and results, Physikalisch-Technische Bundesanstalt (PTB), PTB-N-35, Braunschweig, Germany, 1998.

[27] A. Hildebrand, et al., Experimental Determination of the Response Matrix of a BC501 Scintillation Detector using a Wide Neutron Spectrum: A Status Report, Physikalisch-Technische Bundesanstalt (PTB), PTB-642-05-1, Braunschweig, Germany, 2005.

[28] A. Öhrn, et al., Calibration procedure for a neutron monitor at energies below 20 MeV, Nucl. Instrum. Methods A 592 (2008) 405–413.

[29] T. Novotný, Photon spectrometry in mixed neutron-photon fields using NE213 liquid scintillation detectors, Physikalisch-Technische Bundesanstalt (PTB), PTB-N-28, Braunschweig, Germany, 1997.

[30] M. Zbořil, et al., Simulation of the neutron response functions of diamond detectors with the NRESP code, in: Proc. 1st EPS Conf. Plasma Diagnostics (ECPD2015), Frascati, Italy, 2015.

[31] G.C. Taylor, et al., Accurate simulations of TEPC neutron spectra using GEANT4, Radiat. Phys. Chem. 116 (2015) 186–188.

[32] A.R. Garcia, et al., MONSTER: a time of flight spectrometer for β-delayed neutron emission measurements, J. Instrum. 7 (2012).

[33] T. Martínez, et al., MONSTER: a TOF spectrometer for β-delayed neutron spectroscopy, Nucl. Data Sheets 120 (2014) 78–80.

[34] B. Rubio, DEcay SPECtroscopy (DESPEC) at the new FAIR-NUSTAR facility, Internat. J. Modern Phys. E 15 (2006) 1979–1988.